First passage of molecular motors on networks of cytoskeletal filaments

Paul J. Mlynarczyk and Steven M. Abel*
Department of Chemical and Biomolecular Engineering, University of Tennessee, Knoxville, Tennessee 37996, USA

(Received 7 August 2018; revised manuscript received 21 November 2018; published 11 February 2019)

Molecular motors facilitate intracellular transport through a combination of passive motion in the cytoplasm and active transport along cytoskeletal filaments. Although the motion of motors on individual filaments is often well characterized, it remains a challenge to understand their transport on networks of filaments. Here we use computer simulations of a stochastic jump process to determine first-passage times (FPTs) of a molecular motor traversing an interval containing randomly distributed filaments of fixed length. We characterize the mean first-passage time (MFPT) as a function of the number and length of filaments. Intervals containing moderate numbers of long filaments lead to the largest MFPTs with the largest relative standard deviation; in this regime, some filament configurations lead to anomalously large FPTs due to spatial regions where motors become trapped for long times. For specific filament configurations, we systematically reverse the directionality of single filaments and determine the MFPT of the perturbed configuration. Surprisingly, altering a single filament can dramatically impact the MFPT, and filaments leading to the largest changes are commonly found in different regions than the traps. We conclude by analyzing the mean square displacement of motors in unconfined systems with a large density of filaments and show that they behave diffusively at times substantially less than the MFPT to traverse the interval. However, the effective diffusion coefficient underestimates the MFPT across the bounded interval, emphasizing the importance of local configurations of filaments on first-passage properties.

DOI: 10.1103/PhysRevE.99.022406

I. INTRODUCTION

Active intracellular transport is essential for proper cellular function in eukaryotes, with defects resulting in various types of disease [1]. Passive diffusion is often too slow for transport across cellular distances, so biological cargo such as vesicles and organelles are commonly transported via active processes [2–4]. Active transport is facilitated by molecular motor proteins that bind cargo and generate directed motion along cytoskeletal filaments by converting energy obtained from the hydrolysis of ATP into mechanical work [5–8]. The cytoskeleton of the cell comprises a network of filamentous protein assemblies and serves as a substrate for the movement of motor proteins in the cytoplasm [9,10]. Individual filaments have a polarity that dictates the direction in which a motor protein moves.

Myosins are a class of molecular motors that travel along actin filaments [11]. The organization of the actin cytoskeleton is controlled by many accessory proteins; commonly, it can be found in an approximately random configuration, with little correlation between filaments [12,13]. In traversing a cytoskeletal network, active transport along filaments is interspersed with passive cytoplasmic motion [14]. Although the biophysical properties of many types of myosin motors on single actin filaments have been well characterized [15–20], the influence of various features of the cytoskeletal network on transport is not as well established.

Experimental and theoretical studies have shown that an actin network of sufficient filament density can effectively transport material, with transport controlled by motors switching from one filament to another rather than by means of spontaneous changes in network structure [21–23]. Theoretical studies have demonstrated that intermittency in passive versus active transport can increase the efficiency of transport by decreasing the amount of time required to traverse a given intracellular distance [24,25]. Thus, the spatial organization of the filament network can significantly affect the transport of molecular motors. In addition, the local organization of filaments can have outsized influence on transport over larger length scales. Experimental and theoretical studies have shown that motors can become trapped at junctions of multiple filaments, leading to unproductive cycling states [26,27]. Work related to the statistical physics of traffic phenomena has also provided insight into systems of multiple interacting motors, where bottlenecks can lead to global segregation into high- and low-density regions [28,29].

In the field of stochastic processes, first-passage processes are a class of problems that have been useful in the study of many physical and biological systems [25,30]. Applications in biology include problems involving molecular search, transcription, channel transport, and evolution (reviews of biological applications can be found in Refs. [31,32]). The first-passage time (FPT) is the time to first reach a specific state (or set of states) starting from a specified initial condition. Because FPTs reflect the underlying stochastic process, they provide a useful way to characterize properties of the process and are often directly related to physical properties of interest. For the case of coupled active and passive motor transport, characterizing FPTs gives insight into the timescales and variability of transport. For the example of a motor crossing an interval, a small mean first-passage time (MFPT) and low variability would represent fast and reliable transport; in

*abel@utk.edu

 ©2019 American Physical Society

contrast, a large MFPT and high variability would represent slow, unreliable transport. In this context, Ando *et al.* used simulations to characterize the FPTs of motors moving from the nucleus to the cell surface and determined that the MFPT was largely determined by the total length of all filaments in the system [27].

Recent experimental and theoretical work has shown intriguing coupling between motor transport and the structure of the underlying cytoskeletal network [26,27]. However, much remains unknown about the relationship between configurations of filaments and the large-scale transport of motors [10,33–35]. In this work, we use stochastic computer simulations to study the transport of single motors traversing random configurations of filaments. We systematically vary the number and length of filaments and characterize the first-passage times for a motor to traverse an interval of fixed length. We examine the FPT distributions of select cases and investigate the impact of net filament polarity. For specific filament configurations, we assess the impact of individual filaments by reversing their polarity and determining the change in MFPT; we then compare the location of high-impact filaments with regions of space in which motors spend large amounts of time. Finally, we assess whether the transport of a motor across a domain with many filaments can be treated as a diffusive process with an effective diffusion coefficient.

II. METHODS

A molecular motor is represented as a particle that diffuses, reversibly binds to filaments, and undergoes directed motion when bound to a filament. We consider a single molecular motor as it traverses a two-dimensional rectangular system containing static, fixed-length filaments that are randomly distributed in the system space. The dynamics are described by a continuous-time stochastic jump process.

The system is 20 μm by 5 μm with hard-wall boundary conditions. Filaments are represented as line segments with a fixed directionality for motor motion (we refer to this as the polarity of the filament). The filaments are placed by selecting a random point in the system, extending a line segment of a prescribed length at a random angle, and then assigning a polarity at random. Filaments are truncated if they cross a boundary. The number and length of filaments are both systematically varied. The choice of system size is motivated by plant cells, in which motors often traverse large cellular dimensions ($\sim$10 to $\sim$100 μm) with a third dimension that is substantially restricted ($\sim$1 μm) due to the close proximity of a large vacuole and the cell membrane [36].

When the particle is not bound to a filament, it moves diffusively. In the simulations, the particle attempts to move with a fixed step size (100 nm) at random times. Space is continuous, and the step occurs in a randomly chosen direction. The waiting times between attempted moves of an unbound motor are exponentially distributed with rate $k_{\text{hop}} = 270\,\text{s}^{-1}$. If the particle attempts to move outside of a boundary, the move is rejected and time is incremented. The step size and attempted move rate give a diffusion coefficient of $D = 0.675\ \mu\text{m}^2\,\text{s}^{-1}$. When not bound to a filament, the motor has a binding rate of $k_{\text{on}} = 6\,\text{s}^{-1}$ with each filament located within 100 nm of the particle. This is the approximate size of a myosin motor.

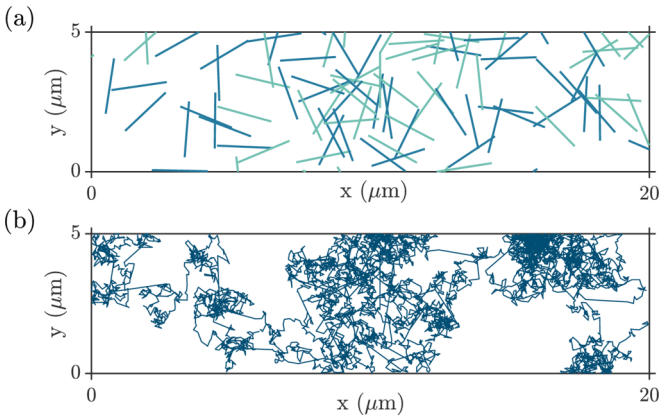

FIG. 1. (a) Random configuration of filaments for a system containing 100 filaments of length 2 μm. Filaments possess either positive (blue) or negative (green) polarity, which specifies whether a motor bound to a filament moves in the positive or negative x direction. (b) Sample path of a motor traversing the system from left to right.

When the motor is bound to a filament, it takes steps of length $\delta = 100$ nm along the filament in the direction prescribed by the filament's polarity. The moves occur at a rate of $k_{\text{fil}} = 60\,\text{s}^{-1}$, giving an average speed of 6 $\mu\text{m}\,\text{s}^{-1}$. The step size in simulations is larger than those measured for myosins ($\lesssim$36 nm), but the average speed on the filament is the important physical property for the simulations [15,16]. The motor unbinds from the filament either spontaneously ($k_{\text{off}} = 2\,\text{s}^{-1}$) or when the end of the filament is reached. The rate constants were chosen to be physiologically relevant and were motivated by *in vitro* experiments with myosin and kinesin [15–17,37]. We use the Gillespie algorithm to generate independent stochastic simulation trajectories using various filament network configurations [38].

The primary quantity of interest is the first-passage time (FPT) for the motor to cross the rectangular interval in the longer (20 μm) dimension, starting from one boundary. The motor starts at the center of the boundary in an unbound state, and the simulation runs until the motor reaches the opposite boundary. The motor crosses the interval by a combination of passive diffusion and active transport along filaments. Figure 1 shows a sample filament configuration along with the path taken by a motor traversing the system from left to right in a sample simulation trajectory. Longer line segments on the path correspond to periods of directed transport. Each independent trajectory results in a different path.

Areas in which the motor spends the most time are characterized by discretizing the system and measuring the time spent in each discrete lattice site. The relative effect of an individual filament on the FPT in a network is investigated by reversing the polarity of that filament and measuring the resulting MFPT.

III. RESULTS AND DISCUSSION

A. First-passage times: Impact of the length, number, and configuration of filaments

We begin by systematically varying the number (N_f) and length (L_f) of filaments in the system. For each case, we

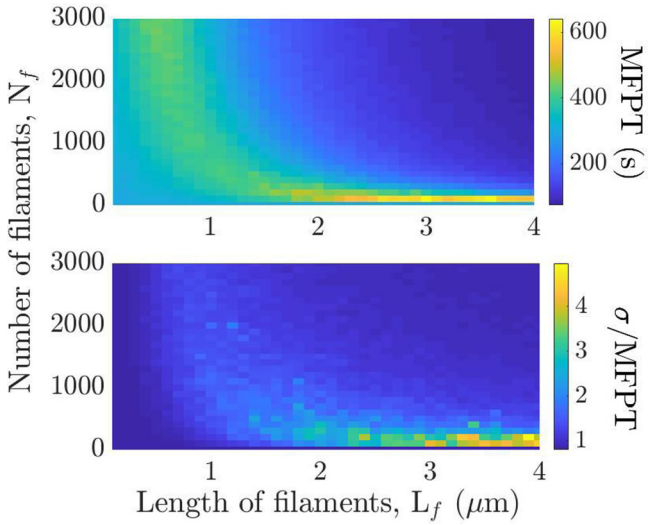

FIG. 2. Mean first-passage time (MFPT, top) and relative standard deviation (σ/MFPT, bottom) for various numbers (N_f) and lengths (L_f) of filaments. Each value is obtained from 10 000 independent trajectories, each generated with a different filament configuration.

generate 10 000 network configurations, each of which is used to obtain a single stochastic trajectory. The mean first-passage time (MFPT) is obtained by averaging the FPTs of these trajectories, and the relative standard deviation is the associated standard deviation (σ) divided by the MFPT.

Figure 2 shows that the largest MFPTs with the highest variability occur in systems containing a relatively small number of long filaments; the smallest MFPTs occur in systems with large numbers of long filaments. Systems with many short filaments also have large MFPTs, but they exhibit less relative variability than systems with relatively few long filaments. It is interesting to note that systems with many short filaments exhibit larger MFPTs than pure diffusion ($N_f = 0$).

Figure 3 shows the full distribution of FPTs for three cases appearing in Fig. 2. This includes the case with no filaments ($N_f = 0$, blue) in which the particle moves by diffusive

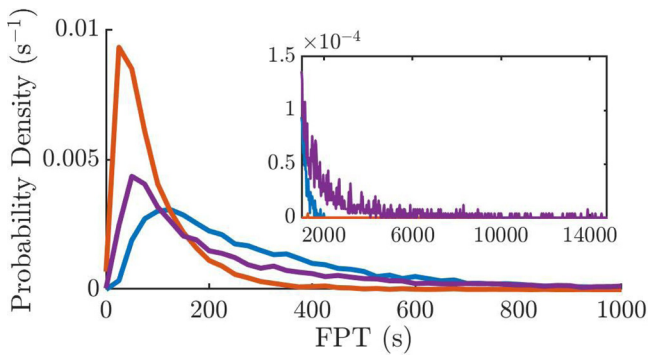

FIG. 3. Probability density of first-passage times (FPTs) in systems with no filaments (blue, MFPT = 298.9 s), 3000 filaments of length 3 μm (red, MFPT = 95.2 s), and 100 filaments of length 3 μm (purple, MFPT = 633.8 s). The tails of the distributions at longer times are shown in the inset. Each distribution is constructed from 10 000 trajectories.

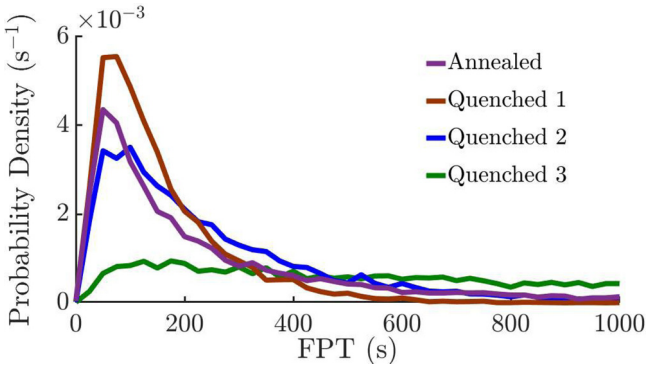

FIG. 4. Annealed versus quenched FPT distributions. The probability density is generated from independent, randomly generated network configurations ("Annealed," MFPT = 633.8 s) and for fixed filament configurations ("Quenched 1–3" for three different configurations; MFPT = 155.7 s, 257.1 s, and 1,111.3 s, respectively). Each network contains 100 filaments of length 3 μm. Each distribution is constructed from 10 000 trajectories.

motion only. The smallest MFPT is associated with large numbers of long filaments ($N_f = 3000$, $L_f = 3$ μm, red). The FPT distribution for this case has a peak at relatively short times and is somewhat right-skewed, with the peak occurring at a time moderately lower than the mean. The case with 100 filaments of length 3 μm (purple) exhibits the largest MFPT. Interestingly, this case has a peak in the FPT distribution at shorter times than the purely diffusive case, but the MFPT is more than twice as long. The large MFPT is caused by the long tail of the distribution in which FPTs are anomalously large but relatively rare (Fig. 3, inset). The overall distribution reflects the time for a motor to traverse many different underlying filament configurations, suggesting that typical configurations lead to relatively fast transport, but that a small fraction of configurations produce very slow transport. Other cases from Fig. 2 with a large relative standard deviation have similar distributions of FPTs.

To investigate the influence of specific filament configurations, we also determine the distribution of FPTs for fixed configurations. When sampling over independent, randomly generated filament configurations, we refer to the resulting FPT distribution as "annealed." The results shown in Figs. 2 and 3 were obtained in this manner. In contrast, when determining the distribution of FPTs for a specific filament configuration, we refer to the distribution as "quenched." Figure 4 compares annealed and quenched FPT distributions for a system consisting of 100 filaments of length 3 μm. Each quenched distribution was obtained using a different filament configuration. Pronounced differences are evident when comparing results for the three configurations and for the annealed case. In particular, the third quenched distribution is strikingly flat with a long tail. The MFPT associated with this configuration is 1111 s, in comparison with 634 s for the annealed case and 156 s for the first quenched configuration. This indicates that the filament configuration, even with the same network properties, can markedly influence the ability of a motor to traverse the system.

Differences between quenched distributions of FPTs result from differences in the configurations of filaments. In

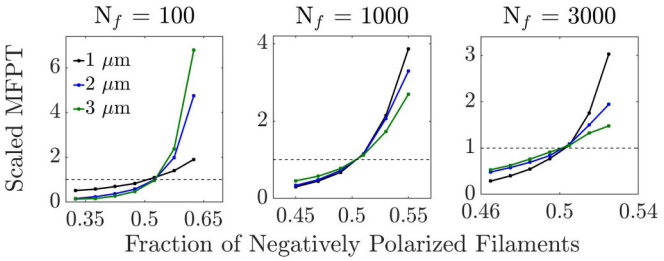

FIG. 5. Scaled MFPT versus the fraction of negatively polarized filaments in the network. Different combinations of filament length (L_f) and number (N_f) are shown. Each curve is constructed with data from 10 000 independent trajectories (each with a randomly generated filament network). For each case, the MFPT for all trajectories is scaled to 1 (horizontal dashed line). The fraction of negative filaments is binned so that each bin contains many samples; the scaled average MFPT for each bin is shown.

the following, we explore both "bulk" properties that reflect the entire filament configuration and "local" properties that involve specific local arrangements of filaments.

B. The MFPT is correlated with net filament polarity

We characterize the net filament polarity of a configuration (a bulk property) as the fraction of negatively polarized filaments. A larger fraction, meaning more filaments are polarized toward the initial boundary, is expected to increase transit times on average because more filaments transport motors away from the target boundary.

Figure 5 shows the MFPT as a function of the net filament polarity for various numbers and lengths of filaments. The dominant trend is that a larger fraction of negatively polarized filaments leads to a larger MFPT, and that relatively small changes in the net filament polarity lead to substantial changes in the MFPT. The results are consistent with trends in Fig. 2: Cases with a larger relative standard deviation (Fig. 2) exhibit a more pronounced increase in MFPT as the fraction of negatively polarized filaments increases. For example, systems with relatively few filaments ($N_f = 100$) exhibit greater sensitivity to the net polarity when filament lengths (L_f) are greater, which is the regime in which they have a large relative standard deviation. In contrast, systems with larger numbers of filaments ($N_f = 1000$ and 3000) are most sensitive to net polarity when filaments are short.

When there is a net filament polarity in the system, the MFPT can be impacted in two ways. The first is that there is a net bias in the transport of the motor across the system. One can think of this as a drift term in a diffusion equation or as a bias in the steps of a random walk. The second is that an increased number of negatively polarized filaments increases the likelihood of local filament configurations that impact the first passage of the motor, for example, by locally trapping the motor in a specific region [26,27] or by acting as a barrier through a particular interval in the system.

C. Identifying traps and high-impact filaments

To probe local effects involving specific arrangements of filaments, we first identify where motors spend the most time

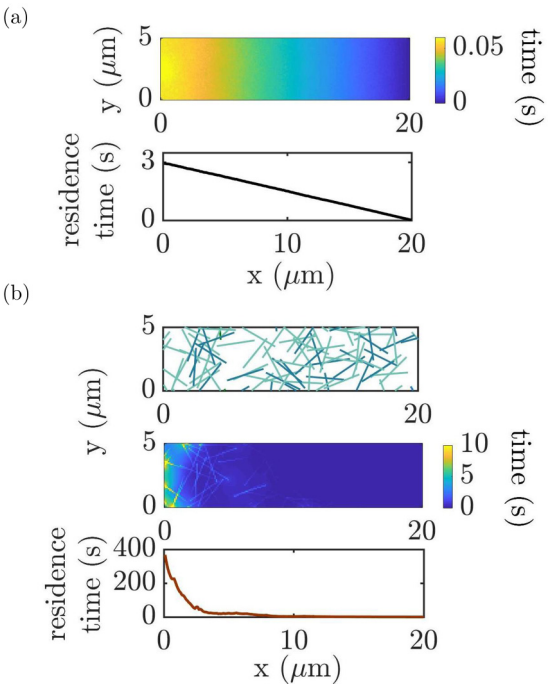

FIG. 6. Average residence times (a) for diffusive motion only (no filaments) and (b) for a fixed filament configuration with $N_f = 100$ and $L_f = 3$ μm (MFPT = 5484 s). The heat maps show the average residence time in each square lattice site when the space is discretized; each site has area 0.01 μm^2. The corresponding line plots show the average residence time in each vertical slice of width $\Delta x = 0.1$ μm. Results are averaged over 10 000 trajectories.

by characterizing the average residence time as a function of position. For a fixed filament configuration, we discretize the system into 0.01 μm^2 square regions and determine the average time spent in each region over 10 000 trajectories.

Figure 6 shows the mean residence time for a system with no filaments and for a fixed filament configuration ($N_f = 100$, $L_f = 3$ μm) with a large MFPT. For the purely diffusive case, the residence time decays from left to right in an approximately linear manner. In general, as in Fig. 6(b), cases with filaments look qualitatively different. Given a filament configuration, the map of residence times highlights the particular filaments and regions of space where a motor spends the most time. Regions with large residence times that are surrounded by small numbers of frequently occupied filaments indicate local filament structures that promote extended occupancy. These filaments constitute a "trap" in which a motor remains confined for extended periods of time [27]. The example in Fig. 6(b) shows that filaments trap the motor near the starting position.

The emergence of traps suggests that small numbers of localized filaments have a disproportionately large influence on the overall MFPT. To probe this idea, we systematically perturb the network structure by reversing the polarity of each filament (one at a time) while keeping all others in their original state. For each perturbed network, we compute the resulting MFPT using 100 independent trajectories. Figure 7(a) shows the results for the filament network presented in Fig. 6(b). The

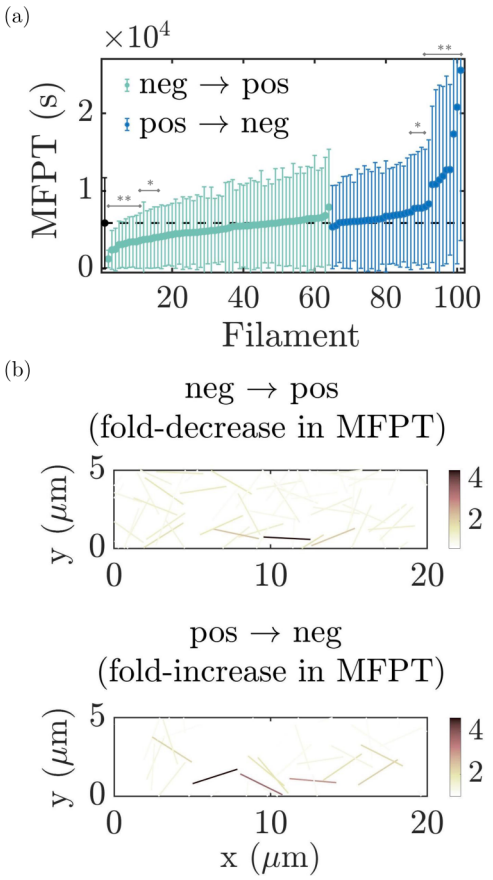

FIG. 7. (a) The MFPT obtained when reversing the polarity of each filament (one at a time) from the configuration in Fig. 6(b). Results are sorted in order of increasing MFPT for filaments that were initially negatively (green) and positively (blue) polarized. The MFPT of each new configuration is averaged over 100 independent trajectories (shown with the standard deviation). The MFPT of the initial configuration is indicated by the dashed horizontal line. Welch's t test is used to test the hypothesis that the MFPT associated with a perturbed filament configuration is equal to the MFPT of the original configuration. Statistically significant differences are denoted by $*$ ($p < 0.05$) and $**$ ($p < 0.01$). (b) Filaments colored according to their impact on the MFPT when their polarity is reversed: The fold decrease in MFPT for filaments changing from negative to positive polarity (left) and the fold increase in MFPT for filaments changing from positive to negative polarity (right).

network contains 100 filaments of length 3 μm, so reversing the polarity of each results in 100 new configurations.

Figure 7(a) shows that changing the polarity of filaments that were initially negatively polarized typically leads to a decrease in MFPT; changing the polarity of filaments that were initially positively polarized typically increases MFPT. The change in MFPT due to a single filament can be quite substantial, as evidenced by the greater than fourfold decrease and fourfold increase in MFPT for the most extreme cases. Using Welch's t test, 30% of the filaments are shown to lead to statistically significant differences in the MFPT when compared with the original configuration. When characterizing the mean residence times for altered configurations, the largest changes are observed around traps.

The previous results suggest that certain filaments have outsized influence on the first-passage properties of motors crossing the interval. The difference in MFPT between the filament with the largest decrease all other cases was statistically significant ($p < 10^{-4}$); the difference between the filament with the largest increase was significantly different ($p < 0.05$) from all but one other case. Given the trap regions previously identified, it is interesting to characterize where the most impactful filaments are located. Figure 7(b) shows the location of filaments and their influence on the MFPT when their original polarity is reversed. Interestingly, the highest impact filaments are not located near the areas of high residence time but instead are found "downstream." In this case, the filaments whose reversal causes the largest increase in MFPT appear to form a bridge that links the trap with a region of the system closer to the final boundary. The other filaments in this region are polarized toward the origin; thus, the high-impact filaments provide the only clear path from one side to the other. When one of them is reversed, the bridge is broken, and the motor is forced to traverse a field of filaments that are polarized toward the origin. Thus, even when the motor exits the initial trap, it is likely to be transported back to the trap. This is conceptually similar to the idea of bottlenecks in the study of traffic [28,29].

This suggests that filaments most critical in determining transit times for a system with a large MFPT are not necessarily those that constitute a trap, but instead can be those providing a path away from one. These filaments act as linchpins connecting different regions and facilitate transport of a motor to or away from areas of prolonged occupancy. This suggests that a motor enters and escapes trapping regions multiple times in a typical trajectory for a filament configuration with a large MFPT, thus producing a recurring unproductive cycling state.

We have focused on a single-filament configuration with a large MFPT. We now consider additional configurations that are characterized by MFPTs that are slow, typical, and fast compared with the annealed average. Figure 8 shows an additional configuration with anomalously slow transport. Traps can again be identified by inspection of the spatially resolved residence times. In this case, the most impactful filament whose reversal leads to an increase in MFPT is located near the end of the trap. The filaments leading to the largest decrease in MFPT are located downstream of the area with large residence time. The next two configurations in Fig. 8 have intermediate MFPTs that are close to the annealed average. These also exhibit areas with enhanced occupancy, but the time spent in these regions is less pronounced than in the slow cases. Flipping individual filaments can still significantly influence the MFPT, but to a lesser relative degree than in the slow cases. High-impact filaments are located both within and downstream of traps. The final two configurations in Fig. 8 have fast MFPTs. In the first, the residence time is relatively constant throughout, in contrast with the diffusive case, which decays linearly. In the second, the motor spends substantially more time in the first half of the domain than the second half. There is a single filament whose reversal leads to a substantial change in MFPT; it is located just beyond the high-residence time area.

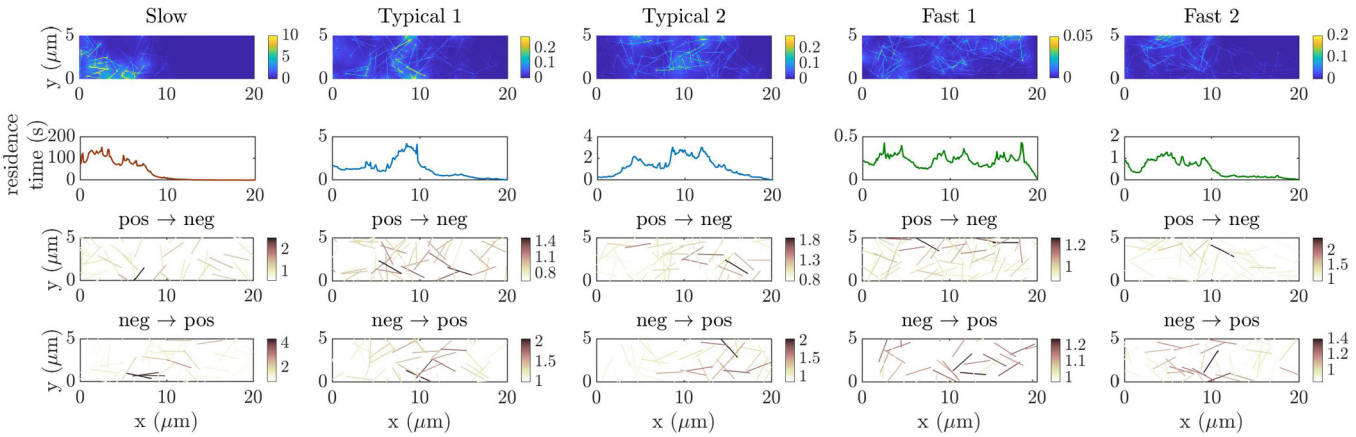

FIG. 8. Residence times and impact of single-filament reversal for five configurations of filaments with $N_f = 100$ and $L_f = 3$ μm. The configurations are categorized as slow, typical, and fast in comparison to the MFPT for the annealed case. From left to right, the MFPT values for the initial configurations are 7960 s, 250 s, 251 s, 46 s, and 98 s. The first two rows show average residence times (analogous to Fig. 6). Rows 3 and 4 show the fold increase and fold decrease in MFPT, respectively, resulting from changing the polarity of single filaments [analogous to Fig. 7(b)].

Collectively, the results in Figs. 7 and 8 show that altering single filaments can dramatically influence the MFPT and that the most impactful filaments can be located in areas that are not associated with traps. For cases in which the high-impact filaments are downstream of traps, they appear to serve as linchpins that connect trap regions with regions further downstream; other filaments in their vicinity are typically polarized in the opposite direction. For anomalously slow FPTs, the physical picture that emerges is that the motor escapes and reenters trap regions multiple times.

D. Do motors behave diffusively when the number of filaments is large?

In the previous section, we focused on a regime with moderate numbers of long filaments. We established that the configuration of filaments plays a large role in dictating FPTs, and that averaging over different configurations leads to broad distributions of FPTs. In this section, we consider a regime with large numbers of filaments. We investigate whether motors behave diffusively in this regime at sufficiently long times, and if so, whether the effective diffusion coefficient produces the MFPT obtained from an annealed average over configurations of filaments.

With a large density of filaments, a motor will spend most of its time bound to filaments because it is typically within binding range of multiple filaments. Additionally, a large density reduces correlations in the motion of a motor imposed by rebinding to recently-traversed filaments. Thus, in a large isotropic system, the motor is expected to undergo a random walk with a step size dictated by the filament length. An effective diffusion coefficient for this motion would be given by $D_e \approx (1/2d)\,\overline{l^2}/\tau$, where $\overline{l^2}$ is the characteristic square distance traveled between each filament binding, τ is the characteristic time to bind and traverse a single filament, and $d = 2$ is the dimensionality. Given sufficiently long filaments, the motor would rapidly bind to a new filament once unbinding from another. Thus, it would spend most time on filaments, and, assuming the dissociation rate of the motor is small, $\overline{l^2}$ would be given by averaging over the square distance from a random binding position to the end of the filament, $\overline{l^2} \approx L_f^2/3$. The characteristic time, $\tau \approx (L_f/2)\delta^{-1}k_{\mathrm{fil}}^{-1}$, is the average time required to traverse half the distance of the filament, giving $D_e \approx L_f\,\delta\,k_{\mathrm{fil}}/6$. Thus, D_e is expected to scale linearly with the filament length for sufficiently long filaments.

To test the whether motors behave diffusively, we calculate the mean-square displacement (MSD) of a motor as a function of time in a larger system (100 μm × 100 μm) with a filament concentration of 20 filaments/μm^2. This is the same filament concentration as for the interval with $N_f = 2000$. We vary the length of filaments and fit the long-time behavior of the MSD to a power law to assess whether it scales linearly in time, as expected for diffusive behavior. Figure 9 shows the MSD for two different filament lengths. The case with short filaments ($L_f = 0.3$ μm) is approximately linear over the entire time domain. The case with long filaments ($L_f = 2$ μm) exhibits superdiffusive behavior at short times (< 1 s) and diffusive

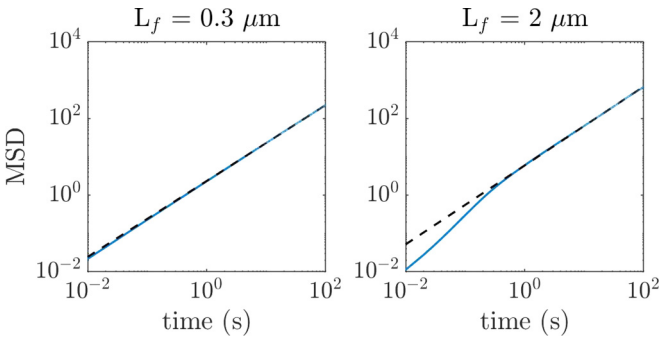

FIG. 9. Mean square displacement (MSD, blue line) of motors in a 100 μm × 100 μm domain with 20 filaments/μm^2. Filament lengths of $L_f = 0.3$ μm (left) and $L_f = 2$ μm (right) are shown. Dashed lines are power-law fits to long-time (10 s < t < 80 s) data obtained from 1000 trajectories of length 100 s. The exponents are 0.99 (left) and 1.03 (right), indicating approximately diffusive motion.

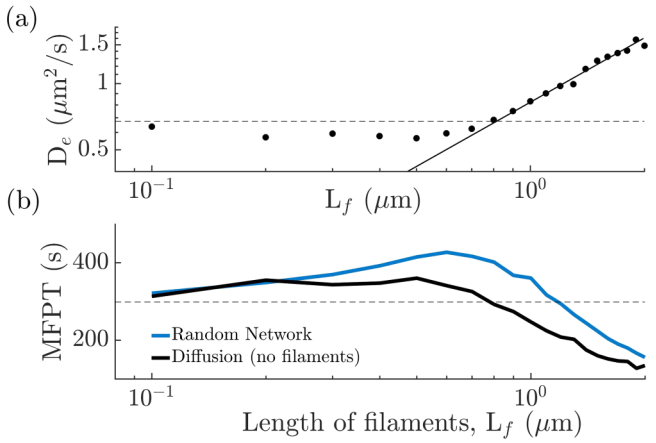

FIG. 10. (a) Effective diffusion coefficient (D_e) obtained from the MSD for various filament lengths (L_f) for a system with 20 filaments/μm^2. The diffusion coefficient of the motor in the cytoplasm is indicated by the dashed line. The solid line is a linear fit to the data ($L_f \geqslant 1$ μm), $D_e = 0.81\,L_f$. (b) Comparison of MFPTs obtained in original simulations with filaments and in simulations without filaments using the effective diffusion coefficient. Cases with a filament network contained 2000 filaments of various lengths. Cases without filaments used the effective diffusion coefficient from (a). All data points represent averages over 10 000 trajectories.

behavior at longer times. This is consistent with ballistic-like motion when motors are bound to filaments and to random-walk behavior at longer times. The diffusive behavior emerges at times considerably shorter than the typical first passage times obtained for a motor crossing a 20 μm × 5 μm interval.

The long-time behavior of the MSD is approximately linear for all values of L_f. We use the slope of linear regime with the expression $\mathrm{MSD}(t) = 4D_e t$ to determine D_e, the effective diffusion coefficient. The results are shown in Fig. 10(a). The diffusion coefficient is nonmonotonic as a function of L_f, as D_e decreases between $L_f = 0$ and $L_f = 0.3$ μm and increases beyond $L_f = 0.3$ μm. This is likely a consequence of short filaments having truncated steps (<100 nm) near the ends of filaments and more frequent rebinding, both of which serve to decrease the effective diffusion coefficient. The behavior of D_e at larger values of L_f increases in an approximately linear manner, which is consistent with the scaling arguments above. However, the slope of the line (≈0.81) is smaller than the value of 1 that emerges from the scaling analysis. This may be because we are not probing sufficiently large values of L_f or because not all of the assumptions (e.g., negligible rebinding) hold. The underlying physics is that, at sufficiently long times, motors undergo random-walk-like motion in which longer filaments lead to larger steps.

We finally determine the MFPT for a motor traversing the original interval (20 μm × 5 μm) in the absence of filaments assuming that it diffuses with the effective diffusion coefficients from Fig. 10(a). The results are shown in Fig. 10(b) (black line). When compared with MFPTs obtained from simulations with explicit filament networks (blue line), it is evident that the effective diffusion coefficient underestimates the MFPT for most filament lengths. Thus, the behavior of the motor in the interval used to obtain FPTs is not well described by purely diffusive motion governed by the effective diffusion coefficient calculated at an equivalent filament density and length. This suggests that local filament configurations impact the FPTs in nontrivial ways. For example, prolonged occupancy of traps is less likely in larger domains because there are more ways to escape them. Thus, in a confined system, filament configurations leading to traps are likely to increase the MFPT relative to that estimated from D_e.

IV. CONCLUSIONS

We used stochastic computer simulations to explore the transport of molecular motors traversing a two-dimensional interval with random configurations of static cytoskeletal filaments. The motors undergo a combination of diffusion in the cytoplasm and active transport when bound to filaments. We varied the length and number of filaments and characterized the mean first-passage time (MFPT) for a motor to traverse the interval. As shown in Fig. 2, cases with relatively small numbers of long filaments had large MFPTs with high variability. This was a consequence of anomalously large first-passage times associated with particular network configurations. Cases with large numbers of short filaments also produced large MFPTs relative to pure diffusion, although with less relative variability. Large numbers of long filaments decreased the MFPT relative to the case of purely diffusive motion. The fact that MFPTs for systems of many short filaments were larger than those for purely diffusive motion suggests that a minimum filament length is needed for active transport to enhance transport across a domain.

We further investigated the source of large, highly variable FPTs, finding that specific filament configurations produced localized spatial "traps" in which motors spend most of their time. Additionally, we systematically perturbed the polarity of each filament to assess the impact on the MFPT. Surprisingly, perturbing certain filaments produced large changes in MFPT. Some of these were found "downstream" of traps, suggesting that high residence times in traps were not only the consequence of the filament configuration in the immediate vicinity, but also of filaments that linked the trap to other spatial regions. These filaments typically provided the only clear path through a region that was otherwise filled with filaments polarized in the opposite direction. This is conceptually similar to well-established results in the statistical physics of traffic showing that bottlenecks can lead to traffic jams, that bottlenecks can be caused by static local properties of the transportation network, and that global segregation into high- and low-density regions can result [28,29]. We also showed that in cases with large numbers of filaments, the mean square displacement of unconfined motors can be used to determine an effective diffusion coefficient. However, this diffusion coefficient underestimates the MFPT to traverse a confined interval, again suggesting the importance of local filament organization when confined in a finite domain.

Overall, we identified general parameter regimes and mechanisms by which intracellular transport of a single molecular motor on a static filament network in two dimensions can become slow and/or unreliable. Many cells have quasi-two-dimensional regions in which motor transport occurs. For example, some plant cells have highly constricted

regions due to the close proximity of a vacuole and plasma membrane. However, understanding transport in less confined regions is also of interest, and extending to three dimensions may reduce the likelihood of traps due to the additional degree of freedom for escape. Additionally, the actin cytoskeleton is regulated by myriad proteins that organize it into structures such as actin bundles [39,40]. It will be of interest to understand effects of actin organization on intracellular transport. In this context, understanding dynamic changes in the cytoskeleton [41–43], crowding effects due to many motors [44–50], and the effects of multiple motors associated with individual cargo [26] will be interesting avenues of future research. This study provides a foundation for investigating these future directions.

ACKNOWLEDGMENTS

This work was supported by National Science Foundation Grants No. MCB-1616495 and No. MCB-1715794. The authors would like to thank Prof. Andreas Nebenführ and Dr. Aaron Prescott for fruitful discussions.

[1] M. Aridor and L. A. Hannan, Traffic **1**, 836 (2000).
[2] D. Arcizet, B. Meier, E. Sackmann, J. O. Rädler, and D. Heinrich, Phys. Rev. Lett. **101**, 248103 (2008).
[3] P. C. Bressloff and J. M. Newby, Rev. Mod. Phys. **85**, 135 (2013).
[4] J. K. Vick and A. Nebenführ, J. Integr. Plant Biol. **54**, 868 (2012).
[5] M. Schliwa and G. Woehlke, Nature (London) **422**, 759 (2003).
[6] R. D. Vale and R. A. Milligan, Science **288**, 88 (2000).
[7] N. Hirokawa, Science **279**, 519 (1998).
[8] B. Gentry, D. Smith, and J. Käs, Phys. Rev. E **79**, 031916 (2009).
[9] J. L. Ross, M. Y. Ali, and D. M. Warshaw, Curr. Opin. Cell Biol. **20**, 41 (2008).
[10] C. Appert-Rolland, M. Ebbinghaus, and L. Santen, Phys. Rep. **593**, 1 (2015).
[11] A. L. Wells, A. W. Lin, L.-Q. Chen, D. Safer, S. M. Cain, T. Hasson, B. O. Carragher, R. A. Milligan, and H. L. Sweeney, Nature (London) **401**, 505 (1999).
[12] C. Loverdo, O. Bénichou, M. Moreau, and R. Voituriez, Nat. Phys. **4**, 134 (2008).
[13] B. Alberts, A. Johnson, J. Lewis, M. Raff, K. Roberts, and P. Walter, *Molecular Biology of the Cell*, 5th ed. (Garland Science, New York, 2008).
[14] H. Higuchi and S. A. Endow, Curr. Opin. Cell Biol. **14**, 50 (2002).
[15] R. Mallik and S. P. Gross, Curr. Biol. **14**, R971 (2004).
[16] J. Howard, *Mechanics of Motor Proteins and the Cytoskeleton* (Sinauer Associates, Sunderland, MA, 2001).
[17] J. M. Ryan and A. Nebenführ, Plant Physiol. **176**, 119 (2018).
[18] L. Samii, G. A. Blab, E. H. C. Bromley, H. Linke, P. M. G. Curmi, M. J. Zuckermann, and N. R. Forde, Phys. Rev. E **84**, 031111 (2011).
[19] A. B. Kolomeisky, J. Phys.: Condens. Matter **25**, 463101 (2013).
[20] C. J. Miller, G. B. Ermentrout, and L. A. Davidson, J. Theor. Biol. **300**, 344 (2012).
[21] A. K. Lewis and P. C. Bridgman, J. Cell Biol. **119**, 1219 (1992).
[22] J. Snider, F. Lin, N. Zahedi, V. Rodionov, C. Y. Clare, and S. P. Gross, Proc. Natl. Acad. Sci. USA **101**, 13204 (2004).
[23] M. Mak, M. H. Zaman, R. D. Kamm, and T. Kim, Nat. Commun. **7**, 10323 (2016).
[24] A. E. Hafner and H. Rieger, Phys. Biol. **13**, 066003 (2016).
[25] O. Bénichou, C. Loverdo, M. Moreau, and R. Voituriez, Rev. Mod. Phys. **83**, 81 (2011).
[26] M. Scholz, S. Burov, K. L. Weirich, B. J. Scholz, S. M. Ali Tabei, M. L. Gardel, and A. R. Dinner, Phys. Rev. X **6**, 011037 (2016).
[27] D. Ando, N. Korabel, K. C. Huang, and A. Gopinathan, Biophys. J. **109**, 1574 (2015).
[28] D. Chowdhury, L. Santen, and A. Schadschneider, Phys. Rep. **329**, 199 (2000).
[29] D. Chowdhury, A. Schadschneider, and K. Nishinari, Phys. Life Rev. **2**, 318 (2005).
[30] S. Redner, *A Guide to First-Passage Processes* (Cambridge University Press, Cambridge, 2001).
[31] T. Chou and M. R. D'Orsogna, in *First-Passage Phenomena and Their Applications* (World Scientific, Singapore, 2014), pp. 306–345.
[32] S. Iyer-Biswas and A. Zilman, in *Advances in Chemical Physics*, edited by S. A. Rice and A. R. Dinner (Wiley-Blackwell, Hoboken, 2016), pp. 261–306.
[33] C. P. Brangwynne, G. H. Koenderink, F. C. MacKintosh, and D. A. Weitz, Trends Cell Biol. **19**, 423 (2009).
[34] M. Stamnes, Curr. Opin. Cell Biol. **14**, 428 (2002).
[35] E. A. Katrukha, M. Mikhaylova, H. X. van Brakel, P. M. van Bergen en Henegouwen, A. Akhmanova, C. C. Hoogenraad, and L. C. Kapitein, Nat. Commun. **8**, 14772 (2017).
[36] J. Verchot-Lubicz and R. E. Goldstein, Protoplasma **240**, 99 (2010).
[37] J. Xu, S. J. King, M. Lapierre-Landry, and B. Nemec, Biophys. J. **105**, L23 (2013).
[38] D. T. Gillespie, Annu. Rev. Phys. Chem. **58**, 35 (2007).
[39] B. Kachar, Science **227**, 1355 (1985).
[40] N. Kamiya, Annu. Rev. Plant Physiol. **32**, 205 (1981).
[41] S. H. Lee and R. Dominguez, Mol. Cells **29**, 311 (2010).
[42] Y.-W. Heng and C.-G. Koh, Int. J. Biochem. Cell Biol. **42**, 1622 (2010).
[43] S. L. Freedman, S. Banerjee, G. M. Hocky, and A. R. Dinner, Biophys. J. **113**, 448 (2017).
[44] M. Weiss, M. Elsner, F. Kartberg, and T. Nilsson, Biophys. J. **87**, 3518 (2004).

[45] S. M. Abel, Y.-L. S. Tse, and H. C. Andersen, Proc. Natl. Acad. Sci. USA **106**, 15142 (2009).

[46] I. Neri, N. Kern, and A. Parmeggiani, Phys. Rev. Lett. **110**, 098102 (2013).

[47] H. Teimouri, A. B. Kolomeisky, and K. Mehrabiani, J. Phys. A: Math. Theor. **48**, 065001 (2015).

[48] H. D. Vuijk, R. Rens, M. Vahabi, F. C. MacKintosh, and A. Sharma, Phys. Rev. E **91**, 032143 (2015).

[49] D. V. Denisov, D. M. Miedema, B. Nienhuis, and P. Schall, Phys. Rev. E **92**, 052714 (2015).

[50] A. Parmeggiani, T. Franosch, and E. Frey, Phys. Rev. Lett. **90**, 086601 (2003).